Preprint - Conference paper

AAG2020
Advances in Architectural Geometry
Ecole des Ponts, Univ. Gustave Eiffel
Champs-sur-Marne, France

Synthesis of kit-of-parts structures for reuse

Jan Brütting, Gennaro Senatore, Alex Muresan, Ioannis Mirtsopoulos, Corentin Fivet

Preprint May 2020
Final paper April 2021

Please cite this article as:

Jan BRÜTTING, Gennaro SENATORE, Alex MURESAN, Ioannis MIRTSOPOULOS, Corentin FIVET, *Synthesis of kit-of-parts structures for reuse*, in O. BAVEREL et al. (eds), Advances in Architectural Geometry 2020, Paris, 2021.

PREPRINT

AAG2020
Advances in Architectural Geometry
Ecole des Ponts, Univ. Gustave Eiffel
Champs-sur-Marne, France

Synthesis of kit-of-parts structures for reuse

Jan Brütting[1,*], Gennaro Senatore[2], Alex Muresan[1], Ioannis Mirtsopoulos[1], Corentin Fivet[1]

[1] Structural Xploration Lab, Swiss Federal Institute of Technology Lausanne (EPFL), 1700 Fribourg, Switzerland

[*] jan.bruetting@epfl.ch

[2] Applied Computing and Mechanics Laboratory, Swiss Federal Institute of Technology Lausanne (EPFL)

Abstract

This paper shows a computational workflow to design a kit of parts consisting of linear bars and spherical joints that can be employed to assemble, take apart and rebuild diverse reticular structures, e.g. gridshells and space frames. Being able to reuse bars and joints among different structures designed with this method reduces the material demand compared to one-off construction. The input of the method is a set of different reticular structures intended to be built from a common kit of parts. In a first step, the structure geometries are optimized such that the structures share groups of members with identical lengths to allow the placement of same bars in all structures. In a second step, the kit-of-parts joints are optimized to allow their reuse in different structures as well. This is achieved by merging the specific connection patterns of nodes from different structures into one joint. The potential of the proposed method is demonstrated via its application to two case studies: 1) the design of three temporary space frame roofs, and 2) the realization of three pavilion-scale prototypes serving as a proof of concept. The latter case study also shows the robotic fabrication of the bespoke joints.

Keywords: kits of parts, structures, reuse, form finding, clustering, space frames, robotic fabrication

1 Introduction

1.1 Motivation

Recent trends in architectural and structural design build on the potential of *reuse* to reduce the environmental footprint of building structures (Iacovidou and Purnell 2016; Gorgolewski 2017). For instance, it has been shown that reusing reclaimed structural elements from obsolete buildings for a second life time avoids raw material use, requires few energy and reduces waste (Fivet and Brütting 2020; Brütting et al. 2020). An alternative approach consists in synthesizing a kit of parts from new materials such that its components are reusable in diverse structural configurations. In other words, multiple structures successively use a common stock of components, which reduces material demand compared to one-off constructions. Although applicable to any building system (Brancart et al. 2017), the strategy is particularly relevant when designing temporary support structures for different uses and sites, e.g. for exhibitions and events.

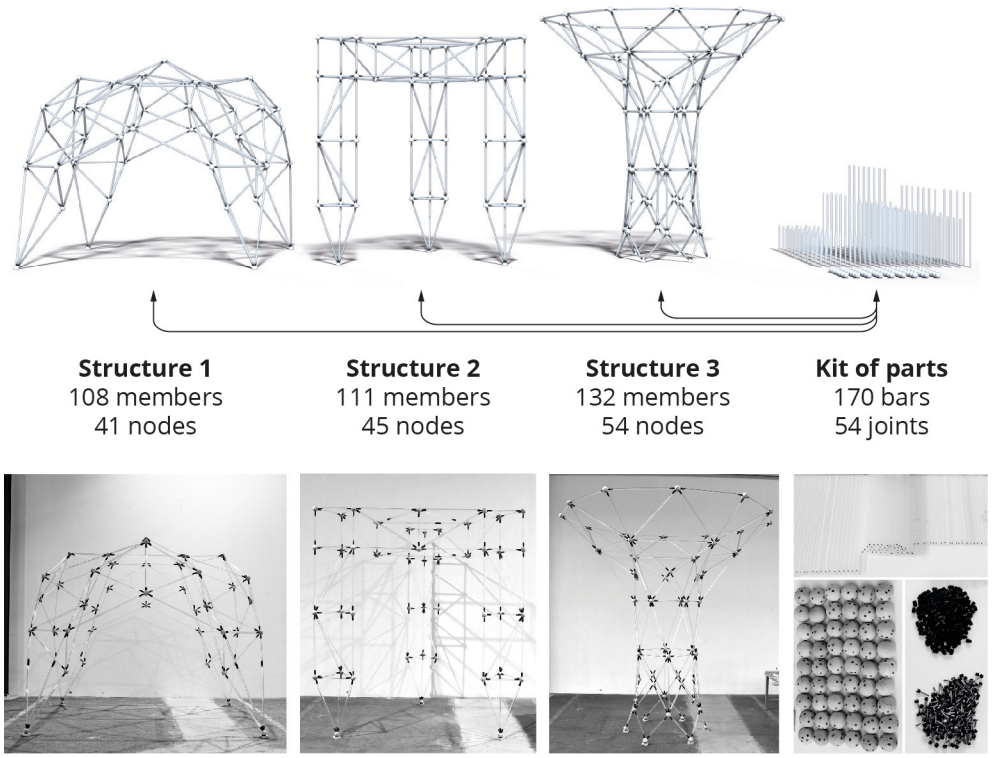

Figure 1: Kit of parts to build three pavilion-scale structures. Because bars and joints are reused among structures, the kit of parts consists of less components than the three structures have in total.

This paper shows a computational workflow to design a kit of parts whose linear bars and spherical joints can be used to build a set of diverse structures, e.g. trusses,

gridshells and space frames. Different to existing solutions, the structure geometries produced by this method are not restricted to repetitive modular arrangements (Figure 1). All connections between parts are reversible to allow for multiple (re-)assemblies.

1.2 Related work

Making complex architectural freeform surfaces and support structures (e.g. roofs or facades) affordable in monetary terms and feasible for manufacturing has been the focus of many architectural geometry *rationalization* methods (Austern, Capeluto, and Grobman 2018). The main driver of these methods is the cost reduction through batch production of identical elements. Following the same motivation, Lobel (1993) showed rules to design a large number of polyhedral surfaces that consist of identical equilateral triangles only. Similarly, Jiang et al. (2015) and Huard, Eigensatz, and Bompas (2014) presented the panelization of freeform surfaces with identical equilateral triangles and Fu et al. (2010) as well as Singh and Schaefer (2010) showed the tiling of surfaces with clusters of triangles and quads. Placing structural members along the edges of panels obtained with these methods gives clusters of members with identical lengths.

An underexplored potential of these sophisticated rationalization methods is that one could apply them to multiple surfaces or structures simultaneously in order to obtain architectural designs where identical elements could be shared among different systems, making possible the reuse of elements.

Typically, modular construction systems are employed when designing and building temporary structures for multiple service cycles. The MERO space frame system composed of tubular linear bars and universal nodal joints is probably the most prominent example. One drawback of the system however is its restriction to certain module geometries such as tetrahedra and octahedra (Mengeringhausen 1975). Following recent advances in architectural geometry modeling and manufacturing, sophisticated construction systems have been developed for more complex freeform reticular structures (Schober 2015; Hassani et al. 2020). However, most parts in these structures remain bespoke to a defined location. Even though it was never the customary objective of these systems, such customization hinders the potential to reuse parts among structures.

In contrast with existing solutions, the method shown in this paper considers the simultaneous design of multiple structures as well as the manufacturing of linear bars and nodal joints such that all parts can be reused in different non-modular structures.

2 Method

In the following the term *member* refers to the link between two *nodes* in a structure. The kit-of-parts *bars* and *joints* are the physical entities that are placed at member and node positions during structure assembly. In general, designing a common kit of parts

for multiple structures implies that all parts have to geometrically fit to positions in different structures and all connections must be reversible to allow multiple (re-)assemblies (Brancart et al. 2017). This section shows the two main steps of the method: 1) the simultaneous form finding of a finite set of structure geometries such that members of identical lengths exist in all structures, and 2) the optimization of the joints to make them fit to nodes in different structures.

2.1 Form finding

The form finding process is summarized on Figure 2. Inputs are the layouts (geometry and topology) of the $s = 1…S$ structures that are foreseen to be built from the kit of parts. First, all $i = 1…m^{tot}$ members of all S structures are clustered into a defined starting number of k^{start} groups based on their member lengths l_i. For the clustering, a univariate *k-means* algorithm (Wang and Song 2011) that is particularly suited for 1-dimensional data (lengths) is employed. The mean length of all members within a cluster c is denoted cluster length l_c, where $c = 1…k$. Next, the node positions of all structures are optimized with the objective to match the member lengths with the length l_c of the cluster to which the members have been assigned through k-means. In this work, a customized implementation of the software *Kangaroo Physics v. 2.42* (K2) (Piker 2020) is employed for the optimization of node positions: for each member a *length goal* (Piker 2016) with the 'rest-length' being l_c is defined. Member length clustering and optimization of structure node positions are iteratively repeated until convergence (close matching of member and cluster lengths). If needed, the number k of clusters is then incrementally increased or decreased until it equals a given k^{end} (Figure 2). k^{end} determines the eventual number of different bar lengths in the kit of parts.

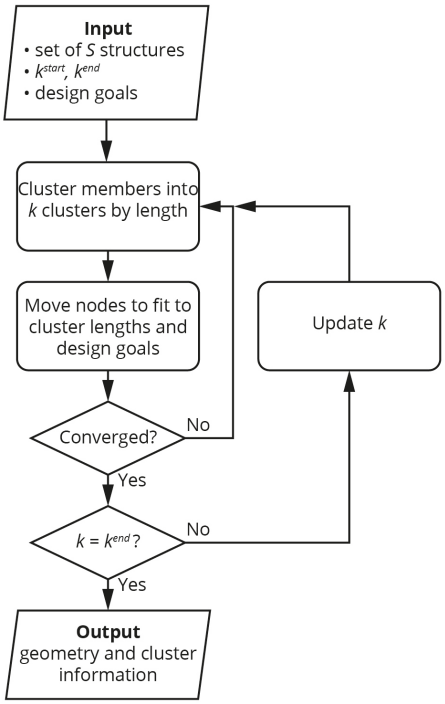

Figure 2: Flow chart of the form finding and member length clustering method.

Figure 3 illustrates the form finding and clustering through an example. The input are two reticular structures with 12 and 11 members respectively (Figure 3a). Member lengths are clustered into k = 3 groups, (Figure 3b). The structure geometries obtained after convergence of the form finding process (Figure 3c) display members with identical lengths in each cluster (Figure 3d). Members of same length can be shared and reused among both structures. Therefore, the kit of parts must contain only as many bars as maximally used in one of the two structures (grey regions in Figure 3d). The number of bars per cluster and length is denoted n_c. In total n_{tot} = 15 bars are required to be able to consecutively build the two structures.

A means to evaluate the performance of a form finding solution is the *homogenization rate* HR, defined as the ratio between total number m_{tot} of members in the two structures and the number n_{tot} of members in the kit of parts. In this example HR = m_{tot}/n_{tot} = 23/15 = 1.53. In general, the aim is to obtain a large HR value meaning that many bars can be reused.

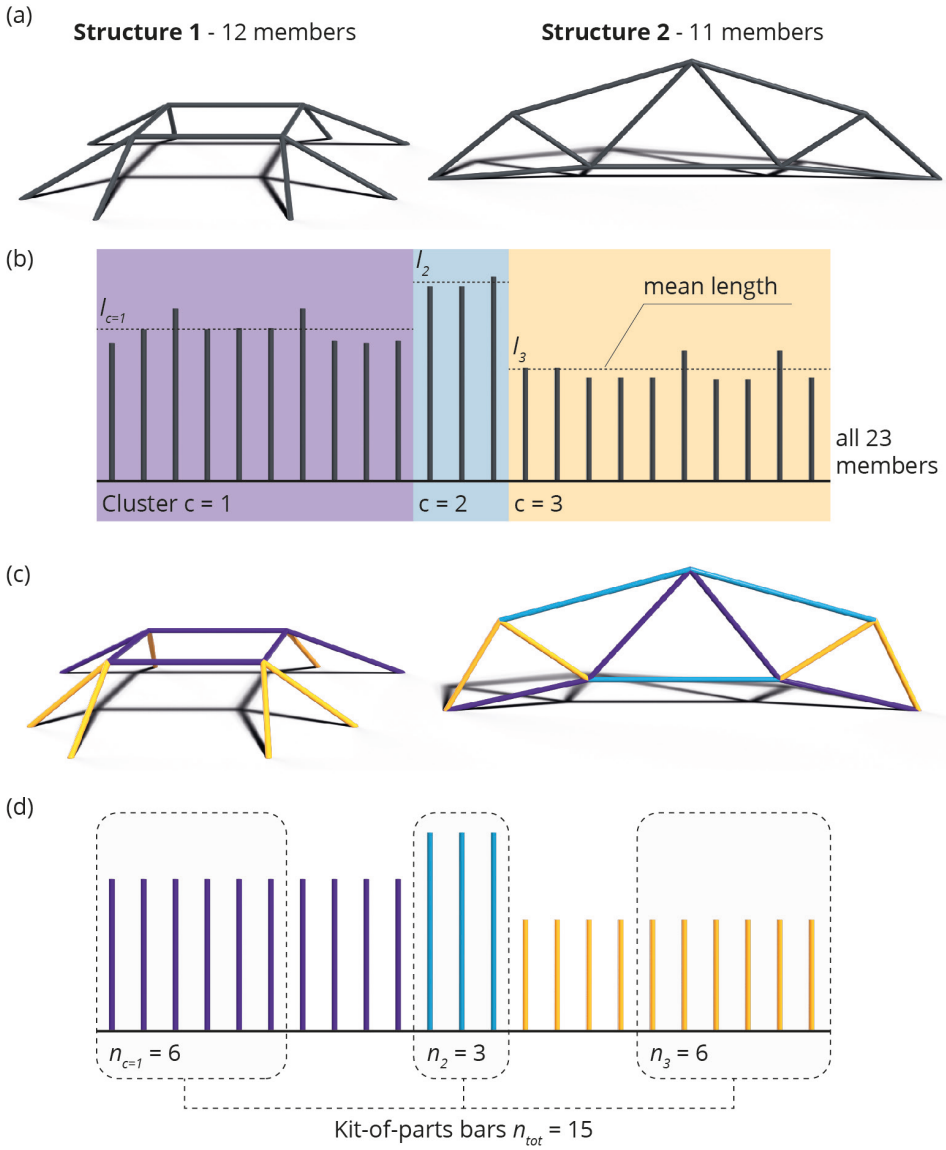

Figure 3: Example application of the form finding method: **(a)** input structure layouts, **(b)** member length clustering into k = 3 groups, **(c)** form-found geometries, and (d) selection of the subsets of members that make up the kit of parts. Cluster colors in **(b)** and members colors in **(c)** and **(d)** correspond.

Throughout the form finding process, it might not always be possible to exactly match member and cluster lengths. In this case the bars need to be manufactured with the length of the shortest member within a cluster. The resulting length difference (or *gap*) between members and bars is denoted Δ. In practice, such gap could be filled with custom *spacers* of specific thicknesses (e.g. 1 mm, 2 mm, …).

The advantage of employing K2 as form finding engine is its potential for combining the clustering of member lengths with many other design *goals* (objectives and constraints), either those that are available in the K2 library (Piker 2020) or custom scripted ones (Piker 2016). In K2, goals are combined using weighting factors *w* and inputs can be parametrically adapted which allows for a user interactive design.

2.2 Joint optimization

This work considers reticular structures in which bars are connected at nodes via spherical joints, fastened together with bolts (Figure 6, section 3.1). The bolts are screwed into holes located on the joint sphere surface. This section presents an optimization method to design joints that fit given node positions in different structures, which allows the reuse of joints among structures.

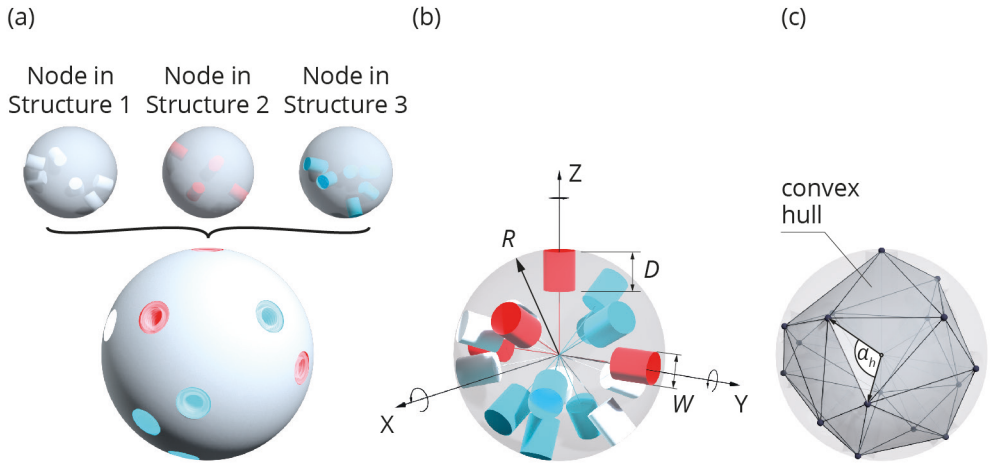

Figure 4: Joint optimization to reuse joints among structures: **(a)** merging of nodes from different structures into one joint, **(b)** rotation of hole sets about the joint central axes, and **(c)** convex hull computed from the hole centers.

Figure 4(a) gives an example of three nodes that are merged into one joint. The *hole sets* that have to be combined in one joint are shown by the red, white and blue cylinders at the top of Figure 4(a). The directions of holes in a set is defined by the directions of the members pointing to the respective node. Placement of holes on the joint is optimized in order to distribute holes evenly over the joint spherical surface. The aim is to avoid locally concentrated perforations and by doing so to increase the mechanical capacity of the joints. In addition, partial overlapping of holes must be avoided. In the optimization, the hole sets are rotated about the joint sphere center as complete entities (Figure 4b) applying the following unconstrained optimization problem:

$$\min_{\boldsymbol{\varphi}} \left(-\frac{1}{R^3} V(\boldsymbol{\varphi}) + \sum_h p(\alpha_h(\boldsymbol{\varphi})) \right) \tag{1}$$

In Eq. 1, the vector $\boldsymbol{\varphi}$ holds the rotations of the hole sets about the X-, Y- and Z axis (Figure 4b). The first term in the objective function maximizes the volume $V(\boldsymbol{\varphi})$ of the convex hull (Figure 4c) which is computed from the centers of each hole. In general, the larger the volume of the convex hull the better the holes are distributed. The factor $1/R^3$, with R being the joint sphere radius, unitizes the volume function. The second term in the objective function is a penalty function meant to avoid partial overlapping of holes. The penalty term p is computed for every central angle $\alpha_h(\boldsymbol{\varphi})$ between a pair h of adjacent holes (Figure 4c). The penalty value varies according to a sinusoidal from 0 when adjacent holes are either superimposed or clearly separated, to 1 when they are in an in-between state:

$$p\big(\alpha_h(\boldsymbol{\varphi})\big) = \begin{cases} 0 & \text{if } \alpha_h(\boldsymbol{\varphi}) > \alpha_{min} \\ sin\left(\frac{\alpha_h(\boldsymbol{\varphi})}{\alpha_{min}}\pi\right) & \text{if } 0 \le \alpha_h(\boldsymbol{\varphi}) \le \alpha_{min} \end{cases} \tag{2}$$

The minimum angle α_{min} that must be respected between two adjacent holes is computed from the joint radius R, the hole depth D and the hole width W (Figure 4b):

$$\alpha_{min} = 2 \cdot \operatorname{atan}\left(\frac{W/2}{R-D}\right) \tag{3}$$

For a fixed hole depth D and width W, the larger the sphere radius R the easier it is to avoid collisions of holes. The optimization problem (Eq. 1) is highly non-linear and non-convex and the computation of a convex hull is non-differentiable. The genetic algorithm of Matlab (The Math Works Inc. 2018) is therefore employed as a solver in this work.

3 Case studies

3.1 Complex space frames

This section shows the application of the method to design a kit of parts for three space frame structures with complex geometry. These structures are thought of as support structures for roofs consecutively installed for temporary events (Figure 5a). Structure 1 is an array of arches over a passage, Structure 2 is an undulating and elongated roof above a stairway, and Structure 3 is a squared roof over a courtyard. Covering of the space frames with panels is out of scope of this study.

Form finding results. Figure 5a shows the input structure layouts considered for the form finding. Only the double-layered space frame parts of the structures and not the support columns that are present in structures 2 and 3 are part of the form finding. The number of bays in each structure (subdivision) has been manually selected such that all members have lengths between 2.00 and 4.60 meters. The three structures contain 420, 320 and 392 members respectively (m_{tot} = 1132). The red dots in Figure 5(a) show the

nodes for which the Z-coordinate has been fixed in the form finding. Next to the member length clustering, two additional design goals are considered in this study: proximity of the structure top layer nodes to the target surfaces, and coplanarity of the nodes located at each edge of the arches in Structure 1 (Figure 5a, blue dots). The weighting factors for the length goal (section 2.1), surface proximity, and coplanarity are denoted by w_L, w_P, and w_C respectively. In general, w_L is chosen orders of magnitude larger than w_P and w_C because matching of member and cluster lengths is a hard constraint to be able to reuse bars. The maximum gap between member and cluster length is denoted Δ_{max}. The average distance of the top layer nodes to their respective target surfaces is denoted ε_{avg}.

In this section, four cases with variation in the number of clusters (k^{end} = 4, 10, 22 and 40) as well as in the weighting factors w_L, w_P, and w_C are studied. Figure 5b-e shows the form found geometries and Table 1 summarizes obtained results for all considered cases. As shown by Figure 5b-e, employing a small number of clusters generally gives structure geometries that are further off from the target shapes. A greater k allows more variation in bar lengths which in turn gives a better proximity of the kit-of-parts solution to the target shape (ε_{avg}).

For case 1) with k^{end} = 4 clusters, the structure geometries are quite regular. For example, Structure 3 only contains members of identical length (purple bars in Figure 5b) and for Structure 2 and 3 the curved appearance of the input is lost. However, this regularity reduces the total number of kit-of-parts bars required to n_{tot} = 456 (HR = 2.50, Table 1) and all members within a cluster have identical lengths (Δ_{max} = 0).

A higher number of clusters (k^{end} = 10) in case 2) gives a smaller homogenization rate of HR = 1.91 and a maximum gap of Δ_{max} = 2.5 mm between bar and member lengths. Table 1 shows the distribution of gap sizes in steps of 0.5 mm. Actually, the gap is 2.5 mm for only three member positions and the majority of gaps is smaller than 1.5 mm. In practice, these numbers refer to the amount of custom spacers that must be placed between bars and joints if such small length differences are not negligible.

In cases 3) with k^{end} = 22 clusters, the curved shapes of the input structures are preserved better. Yet, this comes with a further reduction in homogenization rate to HR = 1.56. The weighting factor w_L is increased to $5{\cdot}10^4$ to obtain a small length gap (Δ_{max} = 0.6 mm). Case 4) has a high number of 40 clusters and serves as a benchmark: to remain close to the input geometry in total 744 bars are required (HR = 1.52).

The rightmost column in Table 1 shows that the computation times for the form finding (obtained on an Intel i7-6820HQ CPU) are small and that an interactive design process for kit-of-parts structures is possible.

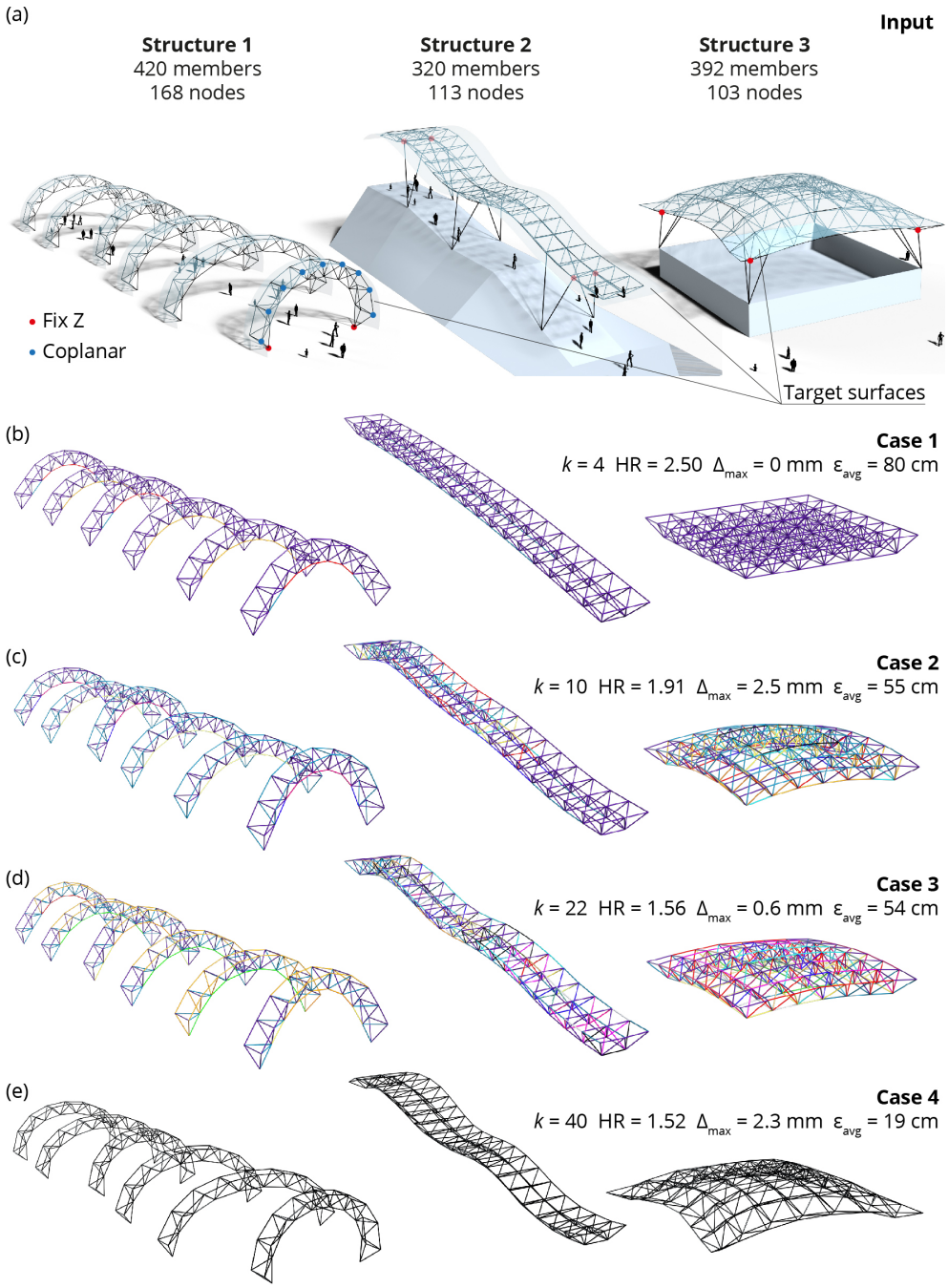

Figure 5: Form finding results: **(a)** input layouts and **(b-e)** results for cases 1) to 4) with variation in the number of clusters *k*; in **(b-d)** members of same color belong to the same length cluster; color mapping in **(e)** is omitted due to the large value of *k*.

Table 1: Form finding results.

case	k^{start}	k^{end}	w_L	w_P	w_C	# bars n_{tot}	HR	Δ_{max}	n|Δ = 0-0.49 mm	n|Δ = 0.5-1.49 mm	n|Δ = 1.5-2.49 mm	n|Δ ≥ 2.5 mm	ε_{avg}	CPU time
	[-]	[-]	$\cdot 10^3$	[-]	[-]	[-]	[-]	[mm]	[-]	[-]	[-]	[-]	[cm]	[s]
1	1	4	10	2	5	456	2.50	0	1132	0	0	0	80	9
2	1	10	10	2	5	594	1.91	2.5	195	453	485	3	55	22
3	1	22	50	2	10	727	1.56	0.6	1099	33	0	0	54	51
4	20	40	80	2	10	744	1.52	2.3	487	604	41	0	19	42

Joint optimization results. The three structures have 168, 113, and 103 nodes respectively (384 in total). Table 2 gives metrics for the initial case where joints are manufactured for a single node and for two optimization cases J1) and J2) following the method shown in section 2.2. J1) decreases the number of joints while J2) decreases the total volume of the joints.

In the initial case, the joint sphere radius can be small (R = 29 mm) because less holes need to fit onto the joint sphere surface. Instead, if multiple nodes are merged into one joint, a larger joint sphere radius is required. As shown by case J1 in Table 2, spheres must have a radius of R = 37 mm to obtain the minimum number of joints (168, i.e. the number of nodes in Structure 1). The total volume V_{tot} of 168 joints with R = 37 mm is 35.6 dm^3, which is 91% of the individual solution with 364 smaller joints (39.2 dm^3). In case J2), only nodes with medium nodal valence are merged in order to avoid difficult distributions of holes. For some nodes with high valence and complex hole sets instead an individual joint is considered. This way in total more joints than in case J1 are required (186) but a smaller radius (R = 33 mm) is possible. The homogenization rate for joints in case J2 is lower but the total volume is reduced to 28.0 dm^3 which is 71% of the initial case.

The results show that material input can be reduced through merging of nodes into reusable joints. In practice, the selection of joint sphere radii might also be constrained by available standard sizes (e.g. R = 30, 35, 40 mm etc.).

Table 2: Joint optimization results

Case	joint radius R	# joints n_{tot}	homog. rate HR	total volume V_{tot}
	[mm]	[-]	[-]	[dm^3]
initial	29	384	1.00	39.2 (100%)
J1	37	168	2.29	35.6 (91%)
J2	33	186	2.06	28.0 (71%)

3.2 Pavilion-scale proof of concept

This section shows the application of the proposed method to the design of three pavilion-scale prototypes (Figure 1). This case study serves as a proof of concept for the proposed method.

Detailing. Figure 6 shows an exploded-view drawing of the joint design and the connector parts used to fasten joints to bars via bolts. The design is inspired by the MERO ball and tube system but adapted to be fully reversible and producible with available fabrication tools. The bars are acrylic glass tubes to obtain a lightweight, transportable structure. The joints are produced from wooden spheres. Holes are drilled into the spheres based on the joint optimization results (section 2.2). To connect bars to the joint sphere via bolts, inserts with an inner and an outer thread are screwed into the holes. Compression forces are transferred from bars to joints through contact of all parts. Resistance in tension between inner tube wall and lid is provided by friction as a rubber pad laterally expands when the bolt is tightened. This way the designed connection is fully reversible and allows multiple assembly cycles. Because the bolt head inside the tube is not accessible, a lock key is inserted through the hex sleeve and a hole in the bolt in order to fasten the bolt from the outside. The mechanical capacity of the connection in tension and compression was sufficient for the pavilion application where small loads are expected. In other applications, different materials such as steel and welded or screwed connections between tubes and intermediate parts should be considered.

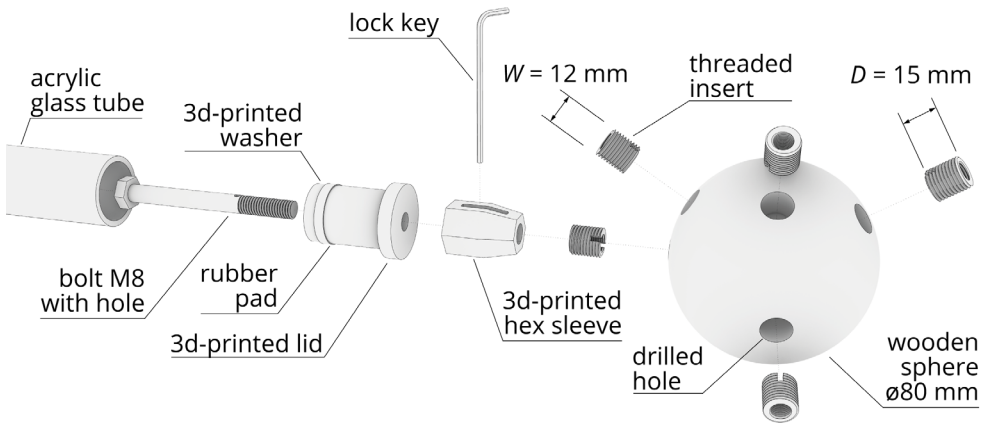

Figure 6: Connection detail of the pavilion prototype.

Form finding and manufacturing of bars. The three input structure geometries are shown at the top of Figure 7. The form finding provided best results with k^{start} = 9 and k^{end} = 6. A computation time ranging between 2.0 to 7.0 seconds allows for the manual adaptation of input layouts as well as interactive addition of design constraints. For instance, upward pointing vertical 'loads' are applied to Structure 1 in order to steer the

form finding towards an inverted hanging model. Figure 7(b) shows the resulting structure geometries that were deemed satisfactory from an aesthetical, reuse and fabrication point of view (Δ_{max} = 0.1 mm). The six different bar lengths are 432, 732, 829, 989, 1126 and 1479 mm. Only n_{tot} = 170 bars are required to build the three structures with a total of 351 members (HR = 2.06, Figure 1).

For the realization of the pavilion structures, the tube cross sections are preliminarily sized based on an adapted version of the optimization method shown in (Brütting, Senatore, and Fivet 2019). A conventional finite element analysis is then employed to verify the cross section sizing and the global stability of the structures. The so obtained cross-section sizes of the bars are ø20/16, ø25/21, and ø30/26 (outer / inner diameter), where bars of larger section are placed at member positions with high demand. Those sizes are also selected to allow the sliding of bars into each other in order to reduce the packaging volume for transport.

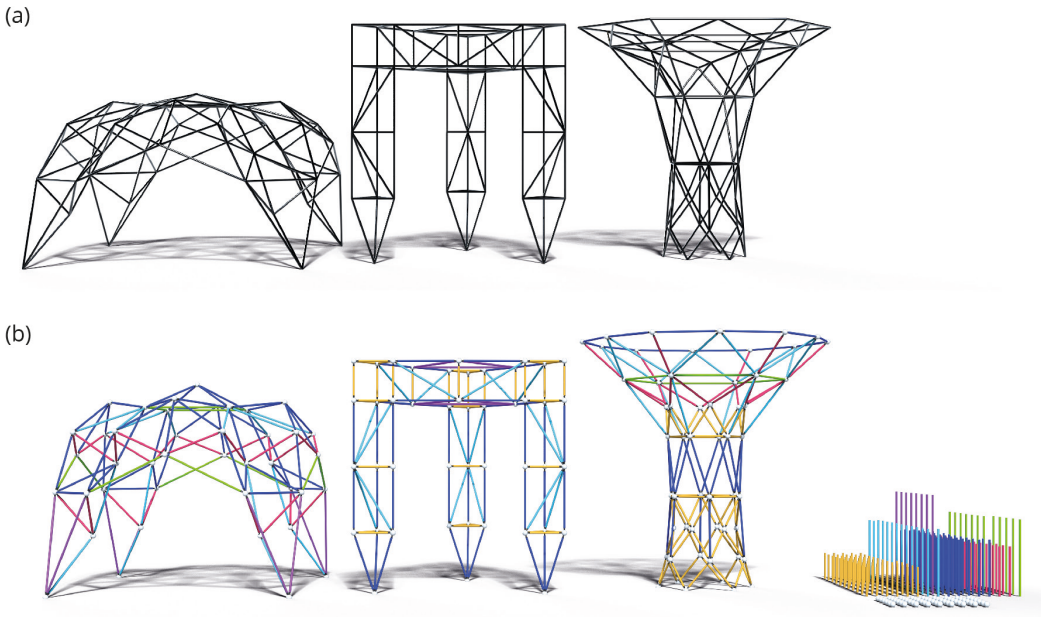

Figure 7: Pavilion case study: **(a)** input structure layouts, and **(b)** form found geometries and kit of parts. In **(b)**, structure members and kit of parts bars of same color have identical length.

Joint optimization and manufacturing. The three structures have 41, 45, and 54 nodes respectively. In order to reduce the number of joints to manufacture, it is decided to merge nodes into the minimum number of joints possible (54), which results in joints with 40 mm radius. If one joint would have been manufactured for each of the 140 nodes individually, a smaller joint sphere radius of R = 37.5 mm could have been used. However, 54 joints with 40 mm radius have only 47% of the material volume of 140 joints with 37.5 mm radius.

After optimal hole directions are obtained via the joint optimization method, joints are manufactured following the steps shown in Figure 8. First, a 'master hole' is manually drilled into each joint sphere (Figure 8a). Then, a threaded insert (Figure 6) is screwed into the master hole to allow the mounting of the joint onto the flange of an industrial robotic arm (Figure 8b). Further, the master hole also determines the orientation of the joint sphere in space. Next, the bespoke hole patterns are drilled into the joints by manoeuvring the joint onto a stationary drill with the robotic arm (Figure 8c).

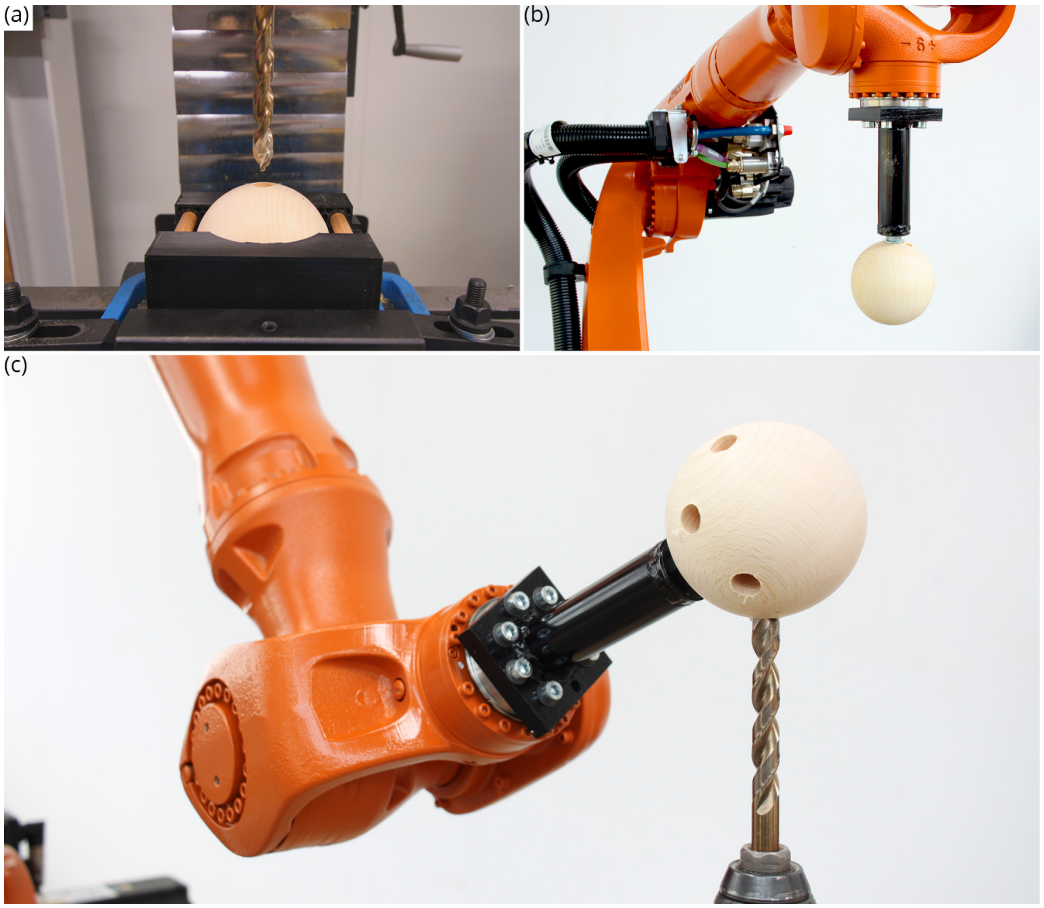

Figure 8: Joint manufacturing: **(a)** Drilling of first 'master hole', **(b)** mounting of joint sphere on robot arm via master hole, and **(c)** drilling of spatial hole pattern via robotic arm and stationary drill.

Kit of parts and assembly. The kit of parts contains 170 bars of six different lengths and 54 spherical joints. Because bolts and intermediate 3d-printed parts are connected to the tubes reversibly, the number of these parts can be even smaller than the total amount of bars. For instance, instead of two bolts per end of the 170 bars, only two times 132 bolts are required in the kit of parts, c.f. maximum number of members in Structure 3. Figure 9 illustrates some of the manufactured and 3d-printed parts as well as the entire kit of parts. Figure 10 shows the prototype structures consecutively

assembled, taken apart and reassembled. The unused holes that can be seen on the assembled joint spherical surface in Figure 11 are used in one of the other structure configurations. The small dots next the holes are encoding the information to which structure a joint hole belongs.

Figure 9: All components of the kit of parts.

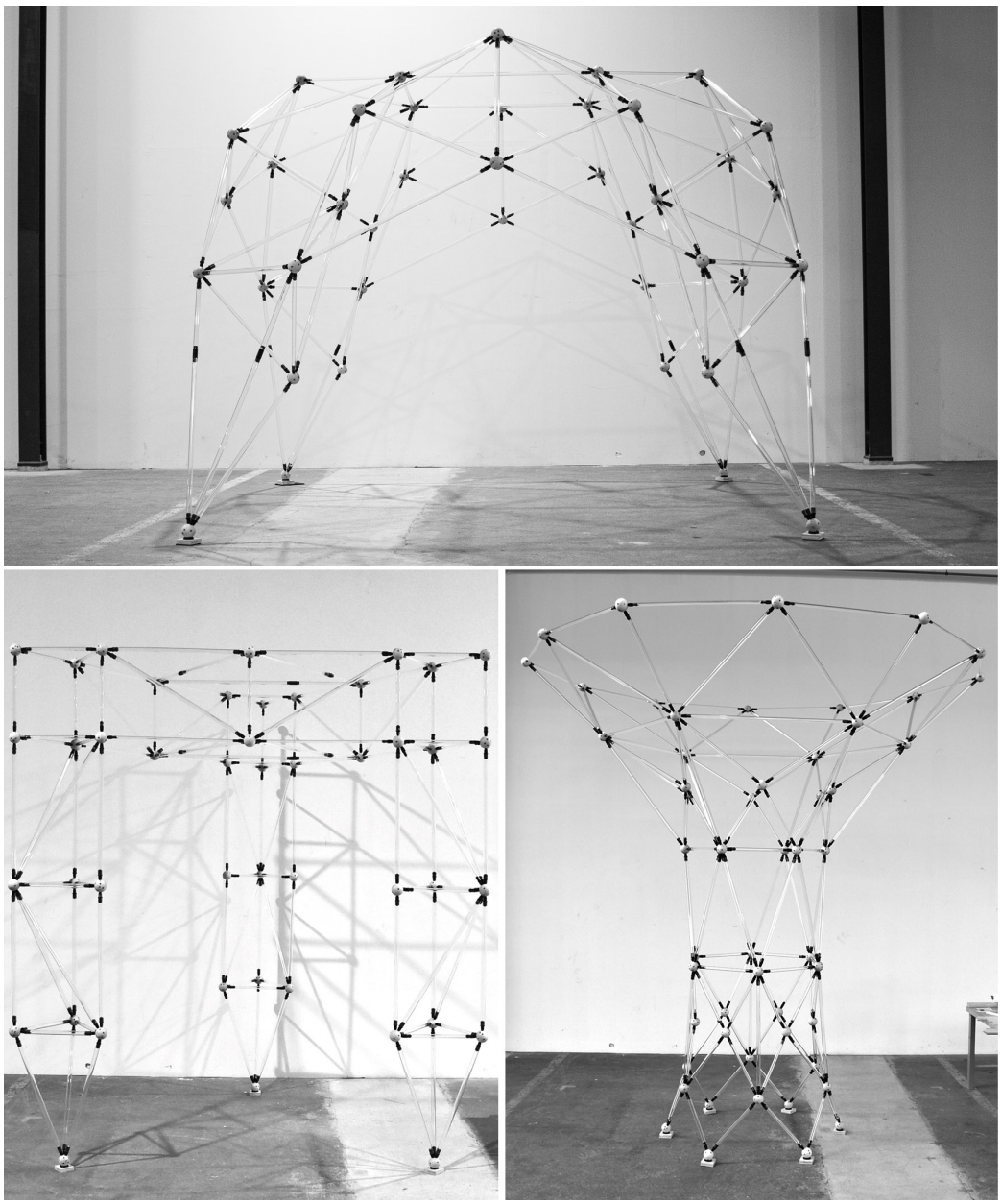

Figure 10: Detailed view of the three assembled pavilion structures.

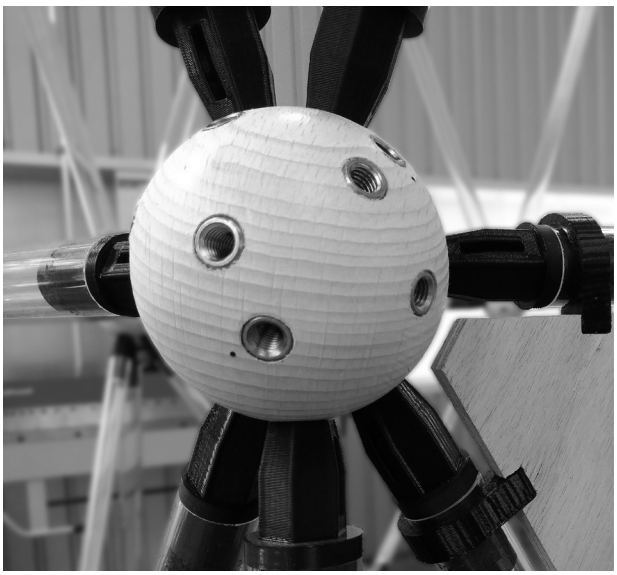

Figure 11: Detailed view of a spherical joint with attached tubes. Unused holes will be used in a different structure assembly.

4 Discussion and future work

From a structural point of view, spherical joints work best in double layer, triangulated structures where they are primarily subject to axial forces. In single layer structures, depending on the loading and structure geometry, the members, joints and centric bolts might be subject to bending moments. Future work could extend the idea of merging multiple nodes into one joint to other joint types such as bending resistant ones.

The focus of this paper was the form finding of structure geometries in order to reuse bars among structures. In general, designing a kit of parts whose components are reused among structures requires considering all load cases that the components experience over all uses (Brütting, Senatore, and Fivet 2019). Future works could study in more detail the simultaneous member clustering and structural geometry optimization.

In this work, a *k-means* algorithm has been employed for member clustering. This method is simple and easy to integrate into the form finding process. However, it requires as input the number of clusters *k*. Future work could study different clustering methods and machine learning techniques to improve the member clustering, of special interest would be those methods where the optimal number of clusters is an output.

In practice, structures require cover panels when used as roofs. Paneling has been out of scope of this work but could be combined with member length clustering in future work in order to allow the reuse of bars and joints as well as panels among structures.

5 Conclusion

This paper shows a novel computational workflow to design and fabricate kit-of-parts linear bars and spherical joints that can be used to build disparate reticular structures. The structures themselves are meant to serve different uses and to be built at different locations. Because the bars and joints geometrically fit to positions in each of the foreseen structures, they can be reused among structures for multiple service cycles. The employed form finding engine further allows for user interaction, fast computations and customization which makes the method suitable as a design tool.

This paper has also shown a novel formulation for optimizing the hole patterns of spherical joints such that these joints can be reused in different structures whilst considering manufacturing constraints.

A proof of concept of the proposed design method has been shown through the realization of three pavilion-scale structures, including the robotic manufacturing of bespoke joints. These prototype structures highlight the potential to extend the method to existing space frame systems and to large-scale practical applications. In addition, a diverse set of structures could be realized with relatively simple and already established fabrication methods. Manufacturing only a subset of elements to build multiple structures might also reduce monetary costs for material input and fabrication compared to one-off construction.

In summary, this paper exhibits how the reuse of parts among different structures opens new research directions for architectural geometry design and rationalization.

Acknowledgments

The authors would like to thank Claude-Alain Jacot, Prateek Kumar, and Cornelius Carl for their dedicated help throughout manufacturing, assembly, exhibition, and documentation of the prototype pavilions. Financial support from Smart Living Lab, KUKA Switzerland, Debrunner, and Opitec for prototyping and manufacturing is thankfully acknowledged.

References

Austern, Guy, Isaac Guedi Capeluto, and Yasha Jacob Grobman. 2018. “Rationalization Methods in Computer Aided Fabrication: A Critical Review.” *Automation in Construction* 90 (June): 281–93. https://doi.org/10.1016/j.autcon.2017.12.027.

Brancart, Stijn, Anne Paduart, Aline Vergauwen, Camille Vandervaeren, Lars De Laet, and Niels De Temmerman. 2017. “Transformable Structures: Materialising

Design for Change." *International Journal of Design & Nature and Ecodynamics* 12 (3): 357–66. https://doi.org/10.2495/DNE-V12-N3-357-366.

Brütting, Jan, Gennaro Senatore, and Corentin Fivet. 2019. "Form Follows Availability - Designing Structures through Reuse." *Journal of the International Association for Shell and Spatial Structures* 60 (4): 257–65. https://doi.org/10.1201/9781315229126-27.

Brütting, Jan, Camille Vandervaeren, Gennaro Senatore, Niels De Temmerman, and Corentin Fivet. 2020. "Environmental Impact Minimization of Reticular Structures Made of Reused and New Elements through Life Cycle Assessment and Mixed-Integer Linear Programming." *Energy and Buildings* 215 (May): 109827. https://doi.org/10.1016/j.enbuild.2020.109827.

Fivet, Corentin, and Jan Brütting. 2020. "Nothing Is Lost, Nothing Is Created, Everything Is Reused: Structural Design for a Circular Economy." *The Structural Engineer* 98 (1): 74–81.

Fu, Chi-Wing, Chi-Fu Lai, Ying He, and Daniel Cohen-Or. 2010. "K-Set Tilable Surfaces." *ACM Transactions on Graphics* 29 (4): 1–6. https://doi.org/10.1145/1778765.1778781.

Gorgolewski, Mark. 2017. *Resource Salvation: The Architecture of Reuse*. Hoboken, NJ, USA: John Wiley & Sons.

Hassani, Vahid, Zubin Khabazi, Hamid Ahmad Mehrabi, Carl Gregg, and Roger William O'Brien. 2020. "Rationalization Algorithm for a Topologically-Optimized Multi-Branch Node for Manufacturing by Metal Printing." *Journal of Building Engineering* 29: 101146. https://doi.org/10.1016/j.jobe.2019.101146.

Huard, Mathieu, Michael Eigensatz, and Philippe Bompas. 2014. "Planar Panelization with Extreme Repetition." In *Advances in Architectural Geometry 2014*, edited by Philippe Block, Jan Knippers, Niloy J. Mitra, and Wenping Wang, 259–79. Cham: Springer International Publishing. https://doi.org/10.1007/978-3-319-11418-7_17.

Iacovidou, Eleni, and Phil Purnell. 2016. "Mining the Physical Infrastructure: Opportunities, Barriers and Interventions in Promoting Structural Components Reuse." *Science of The Total Environment* 557–558 (July): 791–807. https://doi.org/10.1016/j.scitotenv.2016.03.098.

Jiang, Caigui, Chengcheng Tang, Marko Tomičí, Johannes Wallner, and Helmut Pottmann. 2015. "Interactive Modeling of Architectural Freeform Structures: Combining Geometry with Fabrication and Statics." In *Advances in Architectural Geometry 2014*, edited by Philippe Block, Jan Knippers, Niloy J. Mitra, and Wenping Wang, 95–108. Cham: Springer International Publishing. https://doi.org/10.1007/978-3-319-11418-7_7.

Lobel, Alain. 1993. "Lobel Frames." 1993. http://www.equilatere.net/.

Mengeringhausen, Max. 1975. *Raumfachwerke aus Stäben und Knoten: Theorie, Planung, Ausführung*. 7th ed. Wiesbaden: Bauverlag.

Piker, Daniel. 2016. *Dan-Piker/K2Goals*. https://github.com/Dan-Piker/K2Goals.

Piker, Daniel. 2020. "Kangaroo3d." Kangaroo3d. 2020. http://kangaroo3d.com/.

Schober, Hans. 2015. *Transparent Shells: Form, Topology, Structure*. 1st ed. Berlin, Germany: Ernst & Sohn.

Singh, Mayank, and Scott Schaefer. 2010. "Triangle Surfaces with Discrete Equivalence Classes." In *ACM SIGGRAPH 2010 Papers*, 1–7. SIGGRAPH '10. Los Angeles, California: Association for Computing Machinery. https://doi.org/10.1145/1833349.1778783.

The Math Works Inc. 2018. *Matlab R2018a* (version 9.4). The Math Works Inc. https://www.mathworks.com/products/matlab.html.

Wang, Haizhou, and Mingzhou Song. 2011. "Ckmeans.1d.Dp: Optimal k-Means Clustering in One Dimension by Dynamic Programming." *The R Journal* 3 (2): 29–33. https://doi.org/10.32614/RJ-2011-015.